Advances in Science and Technology Research Journal

*Advances in Science and Technology Research Journal*, 2027, 21(1), 522–544
https://doi.org/10.12913/22998624/236277
ISSN 2299-8624, License CC-BY 4.0

Received: 2026.08.02
Accepted: 2026.11.15
Published: 2026.12.01

# Experimental investigation of transient thermal regulation and waste heat recovery mechanisms in a photovoltaic-thermoelectric generator-phase change material hybrid system under tropical outdoor conditions

Indra Hermawan[1,2], Khairil[3*], Akhyar Akhyar[3], Sarwo Edhy Sofyan[3]

[1] Doctoral Program-School of Engineering, Universitas Syiah Kuala, Jl. Tgk. Chik Pante Kulu No. 5 Komplek Universitas Syiah Kuala, Banda Aceh 23111, Indonesia
[2] Department of Mechanical Engineering, Universitas Medan Area, Jl. Kolam No. 1 - Medan Estate, Medan, Indonesia
[3] Department of Mechanical Engineering, Universitas Syiah Kuala, Jl. Syech Abdurrauf No.7 Darussalam, Banda Aceh 23111, Indonesia
* Corresponding author's e-mail: Khairil@usk.ac.id

## ABSTRACT

Waste heat accumulation in photovoltaic (PV) modules can adversely affect electrical performance, while a substantial fraction of absorbed solar energy remains unutilized. This study experimentally investigates the transient thermal response and waste heat recovery of a passive PV–TEG–PCM hybrid system under tropical outdoor conditions. Three configurations, namely conventional PV, PV–TEG, and PV–TEG–PCM, were simultaneously evaluated using identical 30 W monocrystalline PV modules, twenty $Bi_2Te_3$ thermoelectric modules in a 4S5P configuration, an aluminum heat sink, and a paraffin-based phase change material (PCM). The results show that PCM integration increased the maximum measured thermoelectric generator (TEG) temperature gradient from approximately 4.3 to 5.6 °C, corresponding to a 65.77% increase in peak TEG power from 2.56 to 4.24 mW. However, the absolute increase was only 1.68 mW, and the TEG contribution remained below 0.06% of the total electrical output. The effective temperature gradient duration increased from 165.68 to 174.88 min (5.56%), while the cumulative temperature gradient exposure (CTGE) increased from 1023.25 to 1049.75 °C·min (2.59%). Cumulative TEG electrical energy increased from 25.02 to 25.91 J (3.56%), consistent with the higher cumulative temperature-gradient exposure. Stage-dependent analysis showed that the average temperature gradient was 25.95% higher for PV–TEG–PCM during the initial thermal-storage regime but 34.68% lower during the later thermal-response period. These results indicate that PCM primarily modifies the transient thermal pathway by delaying the rise of the TEG cold-side temperature and sustaining favorable temperature-gradient conditions. The effective temperature gradient duration and CTGE are therefore proposed as complementary indicators for characterizing thermal-gradient persistence and cumulative exposure under the tested transient outdoor conditions. Broader applicability requires validation under multiple operating days, weather conditions, PCM properties, and system configurations.

**Keywords:** photovoltaic system, thermoelectric generator, phase change material, waste heat recovery, transient thermal management, effective temperature gradient duration, cumulative temperature gradient exposure.

## INTRODUCTION

The rapid growth in global energy demand and the need to reduce greenhouse gas emissions have accelerated the deployment of photovoltaic (PV) technology as a major component of the renewable-energy transition. PV systems directly convert solar radiation into electricity without operational greenhouse-gas emissions and are increasingly used across residential, commercial,

and utility-scale applications (1, 2). However, only approximately 15–20% of incident solar radiation is converted into electricity, while most of the absorbed energy is released as heat (3, 4). The resulting temperature rise can reduce electrical output and accelerate material degradation (5, 6), with the effects becoming more pronounced under tropical conditions characterized by high irradiance, elevated ambient temperature, and fluctuating meteorological conditions (1, 7). Effective thermal management is therefore required not only to regulate PV operating temperature but also to improve the utilization of otherwise dissipated thermal energy (2, 4).

Various thermal-management approaches have been developed for PV systems. Active techniques, such as forced-air and liquid cooling, can provide substantial temperature reduction but require additional energy, components, and maintenance (4, 8). Passive approaches are consequently attractive because they can regulate thermal behavior without continuous external energy input. Recent experimental studies have demonstrated the potential of different passive or low-energy cooling strategies, including hybrid nanofluid-based backside cooling (9) and outdoor water cooling under realistic meteorological conditions (10). These studies confirm that thermal regulation can influence PV operating temperature and electrical performance, while also highlighting the importance of evaluating thermal behavior under realistic operating conditions. For thermal energy storage, phase change materials (PCMs) can absorb heat during phase transition and delay temperature rise (11, 12), with their effectiveness depending on melting temperature, latent heat capacity, thermal conductivity, and system configuration (12, 13). However, PCM thermal behavior is strongly influenced by the heating and cooling conditions and material properties (14). Because the available storage capacity is finite, the thermal-buffering effect may become less pronounced as the PCM temperature increases beyond its effective phase-transition range (2, 15).

Thermoelectric generators (TEGs) provide a complementary approach by converting part of the temperature difference across their hot and cold sides into electrical energy through the Seebeck effect (11, 16). Their electrical output is strongly dependent on the temperature gradient, $\Delta T$, established across the thermoelectric module (17, 18). Maintaining a favorable $\Delta T$ therefore requires not only sufficient heat at the hot side but also effective control of heat accumulation at the cold side (8, 19). Nevertheless, under practical outdoor conditions, the cold-side temperature can progressively increase, reducing $\Delta T$ and limiting TEG power generation (11, 20). Heat sinks and other cooling strategies have therefore been investigated to improve cold-side heat dissipation (3, 21), although many studies have primarily considered TEG performance at the component level rather than the transient thermal interactions within an integrated PV system (4).

Integrating PCM with TEG offers complementary thermal functions: the TEG provides waste-heat recovery, while the PCM can modify the transient thermal response of the cold-side region through thermal storage (15, 22). Previous PV–TEG–PCM investigations have demonstrated potential improvements in temperature regulation and electrical performance, but many have focused on peak temperature, conversion efficiency, or instantaneous power, and a substantial portion of the reported work has relied on numerical simulations or controlled laboratory conditions (4, 20). Existing transient studies have also examined PCM–TEG systems under dynamic conditions (13, 23), but the persistence and cumulative exposure of the TEG temperature gradient during fluctuating outdoor operation remain insufficiently characterized. Under such conditions, the temperature gradient evolves continuously with irradiance, ambient conditions, heat transfer, and the thermal state of the PCM. Consequently, maximum $\Delta T$ or peak TEG power alone may not fully describe the sustained thermal driving force available for waste-heat recovery (13, 24).

Accordingly, this study investigates the transient thermal and electrical response of a PV–TEG–PCM system under tropical outdoor conditions, with particular emphasis on the evolution of the TEG temperature gradient and its relationship with waste-heat recovery. The study experimentally characterizes the thermal response of the PV rear surface, TEG interfaces, and PCM and evaluates the persistence and cumulative exposure of the measured temperature gradient using the effective temperature gradient duration and cumulative temperature gradient exposure (CTGE). The study further compares these thermal-gradient indicators with the cumulative TEG electrical energy obtained from the measured power response. The contribution is therefore

positioned as a proposed complementary evaluation approach that considers gradient persistence and cumulative exposure alongside conventional instantaneous measurements, rather than as a universally superior metric or established evaluation framework. This approach is intended to provide additional insight into transient heat-flow regulation and TEG energy recovery under the specific outdoor conditions investigated (3, 22, 25).

## MATERIALS AND METHODS

### System configuration and experimental setup

This study developed a hybrid PV–TEG–PCM system that integrates solar energy conversion, waste heat recovery, and thermal energy storage within a single, continuous heat transfer pathway. The overall system configuration is illustrated in Figure 1. Solar radiation incident on the photovoltaic (PV) module is partially converted into electrical energy, while the remaining absorbed energy is dissipated as heat and conducted to the hot side of the thermoelectric generator. The temperature difference established between the hot and cold sides of the TEG generates an electrical voltage through the Seebeck effect. An aluminum heat sink is attached to the cold side of the TEG and is thermally coupled to the phase change material (PCM), which is enclosed within a thermally insulated container. This configuration enables the PCM to provide passive thermal storage and buffering during heating, thereby delaying the temperature rise at the cold side of the TEG and maintaining a favorable temperature gradient during periods of high solar irradiance.

The system incorporates twenty $Bi_2Te_3$ thermoelectric modules connected in a four-series, five-parallel (4S5P) electrical configuration, as illustrated in Figure 2. Each TEG module is separated by thermal insulation to minimize lateral heat transfer, ensuring that heat is transported predominantly along the vertical direction from the PV module, through the TEG, and into the PCM. This arrangement is intended to reduce heat losses caused by lateral conduction, improve temperature uniformity among the thermoelectric modules, and maintain an effective temperature gradient across each TEG, thereby enhancing the overall thermoelectric energy conversion process.

To evaluate the contribution of each component to thermal regulation and waste heat recovery, three system configurations were tested simultaneously under identical environmental conditions: a conventional PV system as the reference configuration, a PV–TEG system, and a PV–TEG–PCM system. In the PV–TEG configuration, the TEG modules were mounted directly onto the rear surface of the PV module using thermal paste as the thermal interface material. In the PV–TEG–PCM configuration, an aluminum heat sink was attached to the cold side of the TEG and thermally coupled to the PCM to establish a passive thermal energy storage system. Thermal paste was applied at the contact

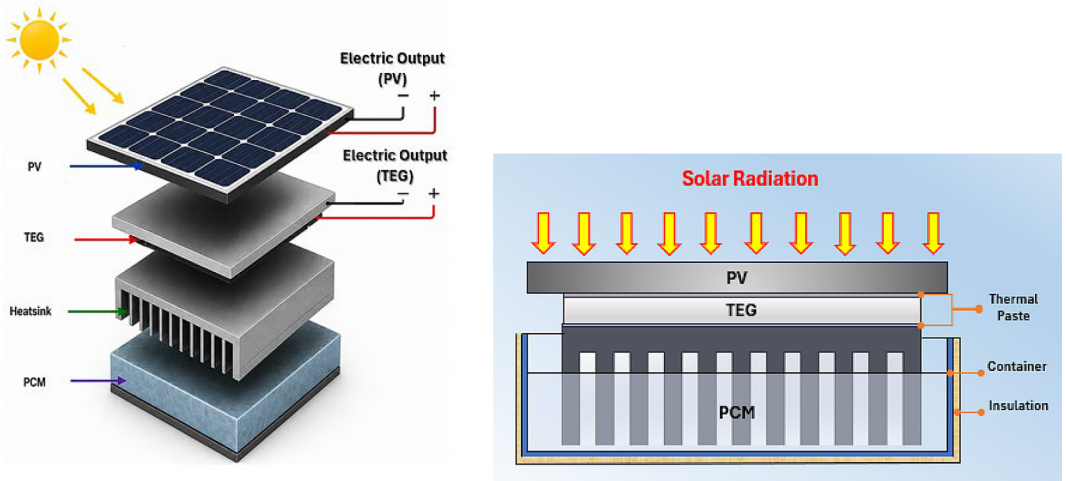



**Figure 1.** (a) Schematic of the PV–TEG–PCM system architecture; (b) cross-sectional configuration of the PV–TEG–PCM assembly

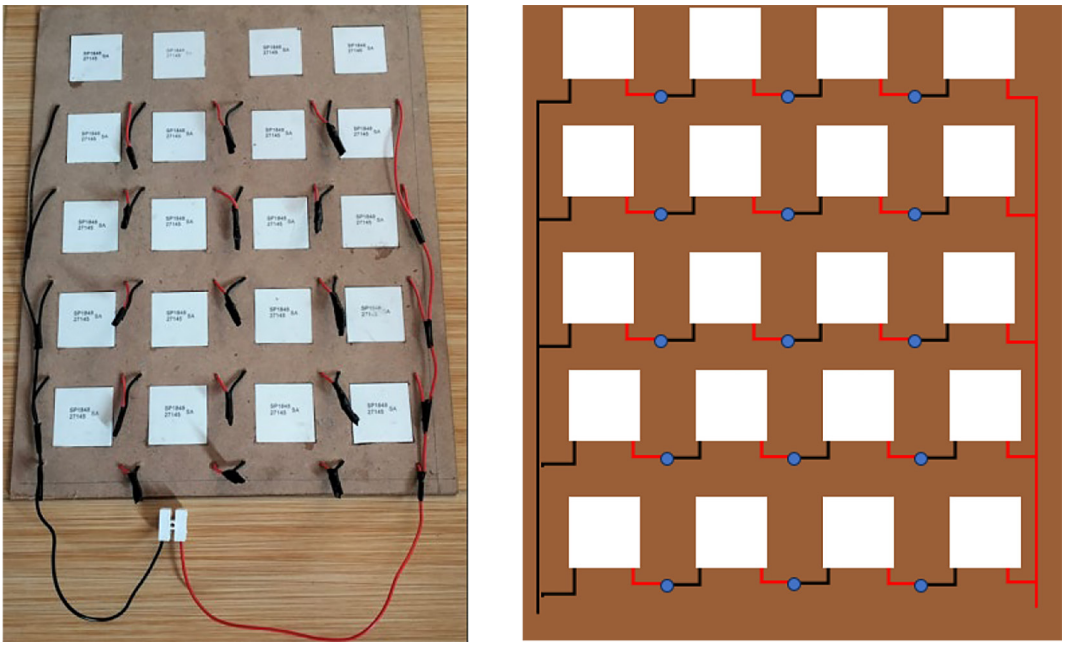


**Figure 2.** Arrangement of the TEG modules in the 4S5P configuration

interfaces to improve thermal coupling and reduce interfacial thermal resistance. However, the thermal paste was not assumed to eliminate the interfacial temperature drop completely. During the experiments, the electrical outputs of the PV module and the TEG were connected to fixed resistive loads of 15 Ω – 100 W and 10 Ω – 20 W, respectively, to maintain consistent electrical loading across the three configurations. Prior to physical modification, the three commercial PV modules were subjected to a pre-modification electrical baseline characterization to ensure comparability of their initial electrical performance. The baseline test was conducted simultaneously under the same tropical outdoor conditions using the same data acquisition system and the same resistive load. The specifications of the energy conversion components and thermal management components used in this study are summarized in Tables 1 and 2.

**Table 1.** Specifications of the energy conversion components

| Components | Description | Value |
|---|---|---|
| Photovoltaic modules | Cell type | Monocrystalline silicon |
| | Maximum power ($P_{max}$) | 30 W |
| | Voltage at $P_{max}$ ($V_{mp}$) | 18.5 V |
| | Current at $P_{max}$ ($I_{mp}$) | 1.63 A |
| | Open-circuit voltage ($V_{oc}$) | 22.0 V |
| | Short-circuit current ($I_{sc}$) | 1.73 A |
| | Outline dimension | 520 × 345 × 25 mm |
| Thermoelectric generator | Model | SP1848-27145 |
| | Material | $Bi_2Te_3$ |
| | Current at 100 °C | 0.669 A |
| | Open-circuit voltage | 4.8 V |
| | Operating temperature | 150 °C |
| | Dimensions | 40 × 40 × 3.4 mm |
| | The Seebeck coefficient | $1.15 \times 10^{-4}$ V/K |
| | The electrical conductivity | $2.52 \times 10^{5}$ S/m |
| | The thermal conductivity | 1.39 W/m·K |

**Table 2.** Thermal management components

| Components | Description | Value |
|---|---|---|
| Heat sink | Material | Aluminium |
| | Dimensions | 40 x 40 x 20 mm |
| | Number of fins | 11 |
| Phase change material | Type | Saturated hydrocarbon (alkane/paraffin-based) |
| | Latent heat | 180–210 kJ/kg |
| | Thermal conductivity | 0.20–0.27 W/m·K |
| | Specific heat (solid) | 2.1–2.5 kJ/kg·K |
| | Specific heat (liquid) | 2.5–3.0 kJ/kg·K |
| | Melting point | ~52 °C |
| | Density (solid, 25°C) | 0.82–0.87 g/cm³ |
| | PCM volume (in container) | ~918 cm³ (0.918 L) |
| | PCM mass* | ~0.75-0.80 kg |
| | Estimated latent heat storage capacity* | ~ 135.5–167.7 kJ |
| PCM containers | Material | Aluminium |
| | Dimensions | 340 x 270 x 10 mm |
| | Thickness | 0.8 mm |

**Note:** *Estimated from the reported PCM volume and material-property ranges; the PCM mass and latent heat storage capacity were not directly measured during the experiment.

All experiments were conducted under tropical outdoor conditions in Deli Serdang, North Sumatra, Indonesia, between 09:30 and 15:30 local time. The three configurations were installed side by side with identical orientation to ensure that they were exposed to the same solar irradiance and environmental conditions. Meteorological parameters, including solar irradiance, ambient temperature, relative humidity, dew point temperature, and wind speed, were monitored continuously to represent the actual operating conditions of photovoltaic systems in tropical environments. The experiment was conducted as a single continuous six-hour test on one measurement day; no repeated trials were carried out on subsequent days.

To characterize the thermal behavior of the PV–TEG–PCM system, Type-K thermocouples were installed at the front and rear surfaces of the PV module, at the PV–TEG interface, at the TEG cold-side/heat-sink interface, within the PCM, and on the outer bottom surface of the PCM container. For the PV–TEG and PV–TEG–PCM configurations, the Type-K thermocouple used to determine the TEG hot-side temperature was positioned directly at the thermal interface between the rear surface of the PV module and the hot side of the TEG. The cold-side thermocouple was positioned at the interface between the TEG and the heat sink. Thermal paste was applied at the contact interfaces to improve thermal coupling and reduce interfacial thermal resistance. Accordingly, the temperature measured at the PV–TEG interface was used as the experimental representation of $T_{hot}$, while the temperature measured at the TEG–heat-sink interface was used as $T_{cold}$. The thermal paste was not assumed to eliminate the interfacial temperature drop completely. The experimental setup and the locations of all temperature sensors are illustrated in Figure 3.

All electrical parameters were recorded using an Arduino Uno R3-based data acquisition system integrated with INA219 sensors for measuring the electrical characteristics of the PV modules and INA226 sensors for measuring the electrical characteristics of the TEG. Temperature measurements were obtained using a Lutron BTM-4208SD temperature recorder connected to Type-K thermocouples. Solar irradiance was measured using a Lutron SPM-1116SD solar power meter, while meteorological parameters, including ambient temperature, relative humidity, and wind speed, were monitored using a WS2320 weather station. The data acquisition system continuously recorded voltage, current, electrical power, and temperature in real time throughout the experimental period. The measurement accuracy of each instrument was considered in assessing the reliability of the

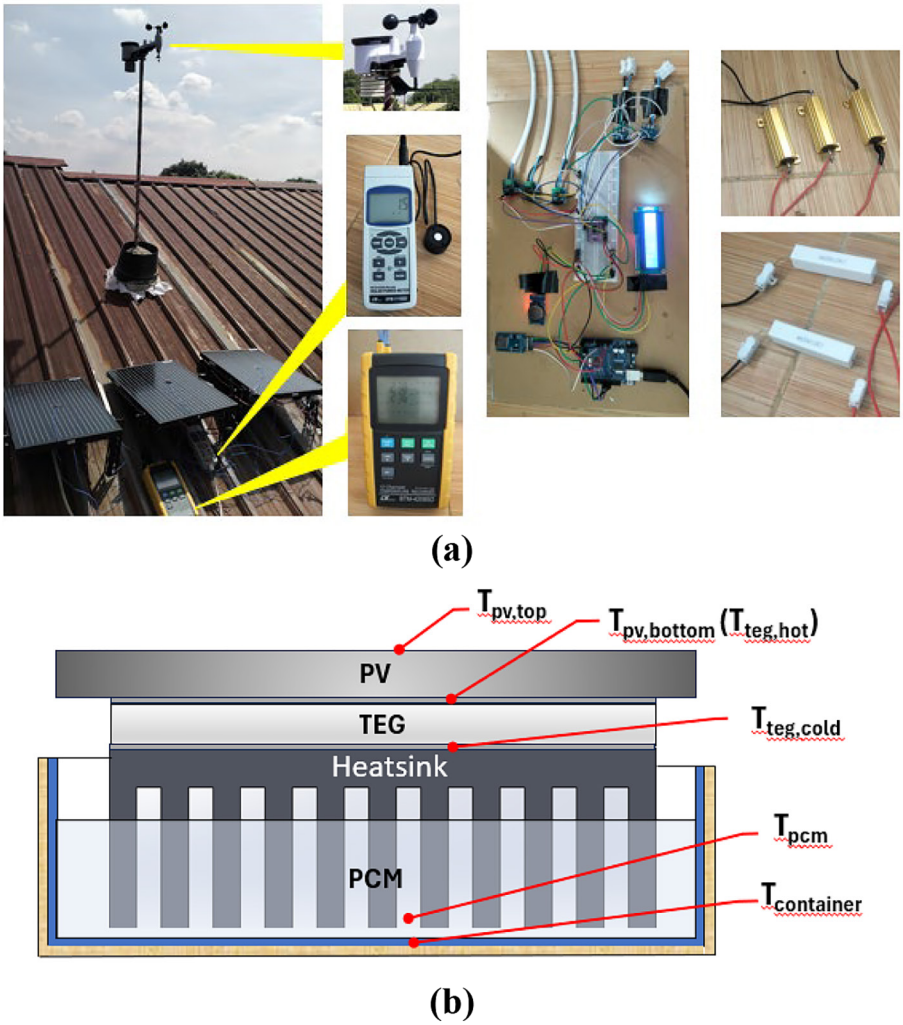



**Figure 3.** (a) Photograph of the experimental system; (b) locations of the temperature sensors

experimental measurements and derived parameters. The corresponding standard uncertainty was estimated from the stated instrument accuracy by assuming a rectangular probability distribution, $u = a/\sqrt{3}$, where $a$ denotes the instrument accuracy limit. For measured quantities used in subsequent calculations, the associated uncertainties were propagated according to their respective mathematical relationships**.** The specifications, measured parameters, stated accuracy, and corresponding standard uncertainty of all measuring instruments used in this study are summarized in Table 3.

## Performance evaluation and data analysis

The performance evaluation was designed to provide a comprehensive assessment of the thermal behavior and electrical characteristics of the three investigated configurations, namely the conventional PV system, the PV–TEG system, and the hybrid PV–TEG–PCM system (4, 25). The analysis focused on the capability of each configuration to regulate the operating temperature of the PV module, sustain the temperature gradient across the TEG, recover waste heat as an additional energy source, and examine the relationship between environmental conditions and system response during outdoor operation (19, 26). This evaluation approach was adopted because the performance of a PV–TEG–PCM system is determined not only by the electrical output of the PV module but also by the dynamic interactions among heat transfer, thermal energy storage, and thermoelectric energy conversion (3, 22).

The electrical performance of the PV module was evaluated using the voltage and current measurements recorded continuously throughout the experimental period. The electrical power output

**Table 3.** Specifications of the measuring instruments and associated measurement uncertainty

| Measuring apparatus | Model | Measured parameter | Accuracy | Standard uncertainty |
|---|---|---|---|---|
| Temperature recorder | Lutron BTM-4208SD | Temperature | Data error ≤0.1% of stored data | According to recorded value |
| Thermocouple | Lutron TP-01 Type-K | Temperature | ±0.4% of reading | $a/\sqrt{3}$ |
| Solar power meter | Lutron SPM-1116SD | Solar irradiance | ±10 W/m² or ±5% of reading, whichever is greater | $a_G/\sqrt{3}$ |
| Weather station | Misol WS2320 | Ambient temperature | ±1°C | $1/\sqrt{3}$ = 0.577 °C |
| | | Relative humidity | ±5% | $5/\sqrt{3}$ = 2.887% |
| | | Wind speed | ±1 m/s (<5 m/s) | $1/\sqrt{3}$ = 0.577 m/s |
| INA219 | PV electrical measurement | PV voltage/current | ±1% of reading | $a/\sqrt{3}$ |
| INA226 | TEG electrical measurement | TEG voltage/ current | ±0.1% of reading | $a/\sqrt{3}$ |

of the PV module was calculated from the fundamental relationship between voltage and current, as expressed in Equation 1 (19, 25).

$$P_{PV} = V_{PV} \times I_{PV} \tag{1}$$

where: $P_{PV}$ is the electrical power output of the PV module (W), $V_{PV}$ is the output voltage of the PV module (V), and $I_{PV}$ is the output current of the PV module (A).

Variations in PV power output were subsequently analyzed in relation to changes in solar irradiance and PV operating temperature to evaluate the influence of thermal conditions on electrical energy conversion performance (4, 26). This approach has been widely adopted in studies of PV–PCM and PV–TEG systems to identify performance degradation associated with increasing module temperature (8, 11). It is important to emphasize that no maximum power point tracking (MPPT) system or periodic I–V characterization was employed in this study. The reported electrical power strictly represents the instantaneous power delivered to a fixed 15 Ω resistive load, rather than the absolute maximum power point (MPP) available from the PV modules. Therefore, comparisons of electrical output are intended to illustrate the system's dynamic electrical response to transient outdoor conditions under an identical load, rather than to determine the intrinsic maximum conversion efficiencies of the PV configurations.

The performance of the TEG was evaluated based on its output voltage, output current, electrical power, and the temperature difference between the hot and cold sides of the thermoelectric module. The electrical power generated by the TEG was calculated using Equation 2 (21).

$$P_{TEG} = V_{TEG} \times I_{TEG} \tag{2}$$

where: $P_{TEG}$ is the electrical power output of the TEG (W), $V_{TEG}$ is the output voltage of the TEG (V), and $I_{TEG}$ is the output current of the TEG (A).

The temperature gradient, which serves as the driving force for the Seebeck effect, was determined using Equation 3 (27).

$$\Delta T_{TEG} = T_{hot} - T_{cold} \tag{3}$$

where: $T_{hot}$ is the hot-side temperature of the TEG (°C), and $T_{cold}$ is the cold-side temperature of the TEG (°C).

The parameter $\Delta T_{TEG}$ was used as the primary thermal indicator for evaluating the effectiveness of the waste heat recovery mechanism because the TEG output voltage is theoretically related to the temperature difference established across the thermoelectric module (3, 18). Accordingly, $\Delta T_{TEG}$ in this study represents the measured temperature difference between the hot-side and cold-side interfaces, rather than the actual thermoelectric junction temperature difference. The relationship between $\Delta T_{TEG}$ and the electrical power generated by the TEG was subsequently analyzed to assess the contribution of PCM integration to maintaining the temperature gradient during the thermal energy storage process (27, 22). The capability of each system to regulate the operating temperature of the PV module was assessed by comparing the PV surface temperatures measured for the three configurations. The effectiveness of thermal regulation was

expressed as the temperature reduction relative to the reference PV system using Equation 4 (4, 25).

$$\Delta T_{PV} = T_{PV,ref} - T_{PV,hybrid} \quad (4)$$

where: $\Delta T_{PV}$ is the reduction in PV module temperature (°C), $T_{PV,ref}$ is the temperature of the reference PV system (°C), and $T_{PV,hybrid}$ is the temperature of either the PV–TEG or the PV–TEG–PCM system (°C).

Beyond evaluating the maximum operating temperature, the analysis also examined the transient temperature profiles throughout the experimental period. This approach makes it possible to assess the capability of the PCM to delay the rate of temperature rise, improve the thermal stability of the system, and mitigate temperature fluctuations caused by variations in solar irradiance (3, 12). Several studies have demonstrated that temperature stability is as important as reducing the maximum operating temperature in improving the reliability of photovoltaic system operation (18, 26).

To quantify the contribution of the TEG to the overall electrical output of the PV system, the total electrical power was calculated as the sum of the power generated by the PV module and that produced by the TEG using Equation 5 (7, 18).

$$P_{Total} = P_{PV} + P_{TEG} \quad (5)$$

The relative contribution of the TEG to the total system power output was subsequently determined using Equation 6 (17, 13).

$$C_{TEG} = \frac{P_{TEG}}{P_{PV} + P_{TEG}} \times 100\% \quad (6)$$

where: $C_{TEG}$ represents the relative contribution of the TEG to the total system power output (%).

Although the electrical power generated by the TEG is relatively small compared with that produced by the photovoltaic module, this parameter remains important for evaluating the potential of waste heat utilization and the effectiveness of integrating the TEG and PCM as a supplementary energy recovery system for photovoltaic applications (22, 23).

To quantitatively evaluate the effectiveness of the temperature gradient beyond its instantaneous peak value, this study introduces two operational metrics, namely the effective temperature gradient duration ($t_{\Delta T,eff}$) and the cumulative temperature gradient exposure (CTGE). These metrics were employed to evaluate the ability of the system to sustain the temperature gradient required for thermoelectric energy conversion throughout the experimental period (27, 3). Effective temperature gradient duration ($t_{\Delta T,eff}$), is used to quantify the effective operational duration of the TEG when the temperature gradient is above the threshold value ($\Delta T_{th}$). This parameter was calculated using Equation 7.

$$t_{\Delta T,eff} = \sum_{i=1}^{n-1} (F_i \times \Delta t_i) \quad (7)$$

where: $t_{\Delta T,eff}$ is the effective temperature gradient duration (min), $\Delta t_i$ is the data acquisition interval (5 min), and the effective interval fraction ($F_i$) is determined based on the following conditions:

$$F_i = \begin{cases} 1, & \Delta T_{TEG,i} \geq \Delta T_{\text{th}} \text{ and } \Delta T_{TEG,i+1} \geq \Delta T_{\text{th}} \\ 0, & \Delta T_{TEG,i} < \Delta T_{\text{th}} \text{ and } \Delta T_{TEG,i+1} < \Delta T_{\text{th}} \\ \dfrac{\Delta T_i - \Delta T_{\text{th}}}{\Delta T_i - \Delta T_{i+1}}, & \Delta T_{TEG,i} \geq \Delta T_{\text{th}} > \Delta T_{TEG,i+1} \\ \dfrac{\Delta T_{i+1} - \Delta T_{\text{th}}}{\Delta T_{i+1} - \Delta T_i}, & \Delta T_{TEG,i} < \Delta T_{\text{th}} \leq \Delta T_{TEG,i+1} \end{cases}$$

where: $\Delta T_{TEG,i}$ is the TEG temperature gradient at the $i$-th measurement point (°C), and $\Delta T_{th}$ is the threshold temperature gradient (°C).

In the present study, $\Delta T_{th}$ was set to 3.0 °C, which closely corresponds to the combined average temperature gradient of the two system configurations over the entire experimental period. The threshold value was determined using a data-driven approach, thereby enabling an objective and unbiased comparison between the investigated configurations.

In addition to the effective temperature gradient duration, this study also evaluated the Cumulative Temperature Gradient Exposure (CTGE) to represent the cumulative thermal driving force experienced by the TEG throughout the experimental period (3, 27). The CTGE was calculated using the trapezoidal integration method, a numerical integration technique for determining the area under the curve from discrete transient measurement data that has been widely adopted in thermal analyses and time-dependent energy system performance evaluations (28, 29). The CTGE is expressed by Equation 8.

$$CTGE = \sum_{i=1}^{n-1} \left( \frac{\Delta T_{TEG,i} + \Delta T_{TEG,i+1}}{2} \right) \Delta t_i \quad (8)$$

where: $CTGE$ is the cumulative temperature gradient exposure (°C·min), $\Delta T_{TEG,i}$ and $\Delta T_{TEG,i+1}$ denote the TEG temperature gradients at two successive measurement points (°C), and $\Delta t_i$ is the time interval between these measurements (min).

Both metrics were calculated for the PV–TEG and PV–TEG–PCM configurations using TEG temperature gradient data recorded at 5 min intervals over the 6 h experimental period (09:30–15:30 local time; $n = 73$ data points). Consequently, the effectiveness of waste heat recovery can be evaluated not only from the maximum temperature gradient attained but also from the ability of the system to sustain that temperature gradient throughout operation (13, 27). While $t_{\Delta T,eff}$ quantifies the duration during which the temperature gradient remains above the prescribed threshold, CTGE characterizes the cumulative exposure to the temperature gradient over the entire experimental period. The combined application of these two metrics provides complementary information for assessing waste heat recovery potential under transient operating conditions (3, 13). To further evaluate the relevance of the measured temperature-gradient exposure to thermoelectric energy recovery, the cumulative TEG electrical energy was calculated by numerically integrating the measured TEG electrical power over the same experimental period using the trapezoidal rule:

$$E_{TEG} = \sum_{i=1}^{n-1} \frac{P_{TEG,i} + P_{TEG,i+1}}{2} \Delta t_i \quad (9)$$

where: $E_{TEG}$ is the cumulative TEG electrical energy (J), $P_{TEG,i}$ and $P_{TEG,i+1}$ are the measured

TEG electrical power at two consecutive measurement points (W), and $\Delta t_i$ is the corresponding time interval (s). In this study, the measurement interval was 5 min (300 s). The cumulative TEG electrical energy was calculated over the same experimental period as CTGE and subsequently compared with CTGE to examine their consistency under transient outdoor conditions.

## RESULTS AND DISCUSSION

### Outdoor environmental conditions during experimental testing

The variations in meteorological conditions throughout the experimental period are presented in Figure 4, while their statistical summary is provided in Table 4. Solar irradiance fluctuated between 323.4 and 1080.7 W/m², reaching its maximum value at 11:20 local time. These fluctuations were accompanied by an increase in ambient temperature from 30.8 to 36.2 °C, whereas the relative humidity decreased from 71% to 52%. Wind speed ranged from 1.3 to 6.3 km/h, with an average value of approximately 3.9 km/h. Over the entire experimental period, the average solar irradiance was 751.7 W/m², while the mean ambient temperature reached 34.2 °C, indicating that the system operated under a high thermal load while experiencing continuously varying solar irradiance caused by intermittent cloud cover, a characteristic feature of tropical climates.

The combination of high solar irradiance, elevated ambient temperature, and low wind speed created conditions that were unfavorable for heat dissipation through natural convection. Consequently, a substantial fraction of the absorbed solar energy that was not converted into electricity accumulated as heat, causing the thermal state of the system to evolve continuously throughout the experimental period (3, 19). In contrast to previous studies, which have predominantly relied on numerical simulations or laboratory experiments conducted under relatively constant irradiance and temperature conditions (22, 27), the present investigation was performed under actual tropical outdoor conditions with representative variations in solar irradiance. This experimental approach enables a more comprehensive evaluation of the transient thermal response of the system by monitoring changes in PV module temperature, the thermal evolution of the PCM, and the development of the temperature gradient across the TEG, thereby allowing the thermal interaction mechanisms under dynamically varying heat loads to be examined under realistic operating conditions (7, 26). These meteorological conditions also provide an appropriate basis for evaluating the capability of the system to manage waste heat, maintain the temperature gradient across the TEG, and preserve thermal stability throughout transient operation (3, 25).

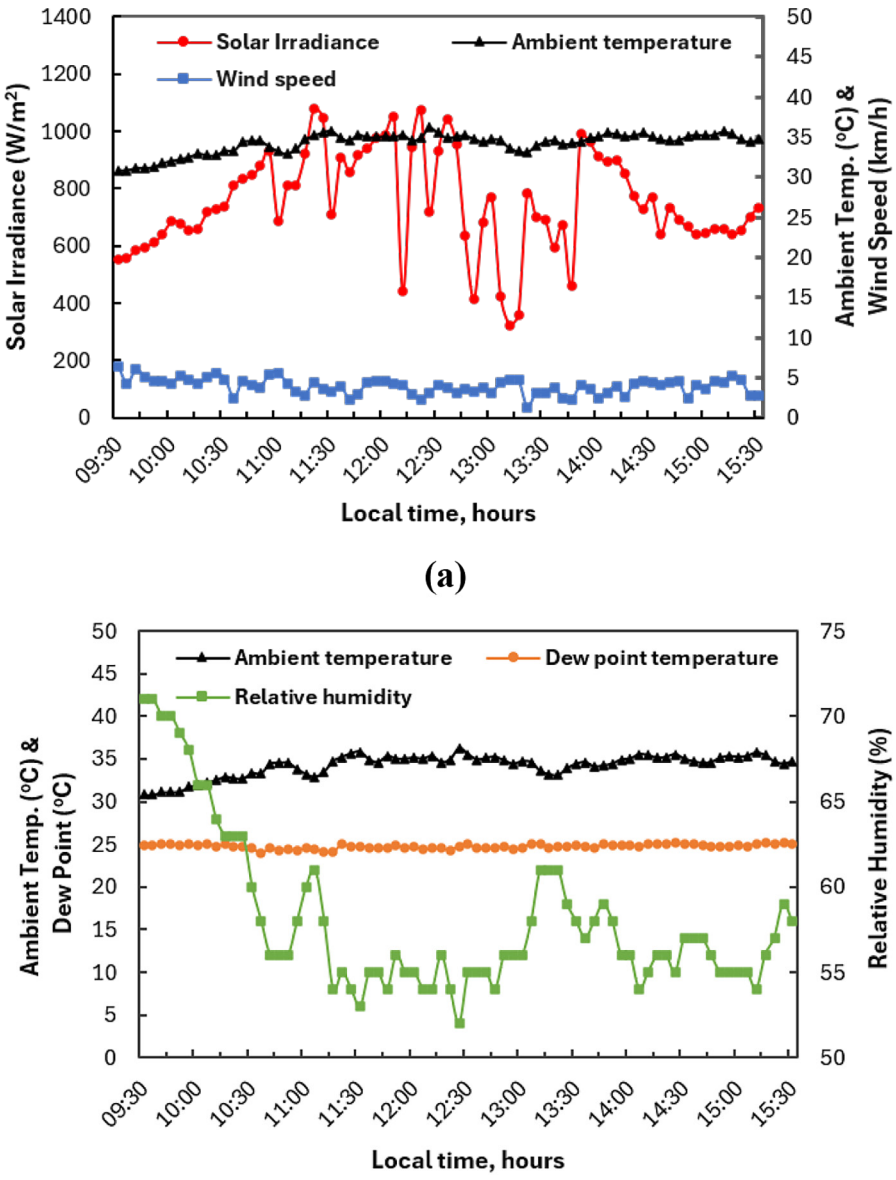



**Figure 4.** Outdoor environmental conditions: (a) solar irradiance, ambient temperature, and wind speed; (b) relative humidity, dew point temperature, and ambient temperature

## Thermal regulation performance of the PV–TEG–PCM system

The comparison of PV module surface temperatures is presented in Figure 5. All configurations exhibited similar transient responses, with temperatures increasing with solar irradiance, reaching their maxima during peak irradiance, and subsequently decreasing as irradiance declined, indicating that PV operating temperature was primarily governed by absorbed solar energy.

For the conventional PV configuration, the front-surface temperature increased from 45.7 °C to 60.1 °C at 12:05 local time, compared with 62.5 °C at 12:25 for PV–TEG and 61.9 °C for PV–TEG–PCM. Thus, PCM integration did not substantially reduce the peak module temperature relative to PV–TEG, although it produced a more gradual thermal response during high irradiance. The PV–TEG–PCM rear-surface temperature increased from 45.4 to 59.4 °C, while the PCM temperature increased more gradually from 41.2 to 55.5 °C, indicating a thermal-storage and buffering effect. Because the PCM temperature approached and exceeded its nominal melting temperature, latent heat absorption may have contributed to this response; however, the present measurements do not directly quantify the sensible and latent heat contributions.

Quantitatively, the reduction in the rear-surface temperature of the PV module relative to the reference system $\Delta T_{PV}$ was determined using

**Table 4.** Summary of outdoor environmental conditions during experimental testing

| Parameter | Minimum | Maximum | Average |
|---|---|---|---|
| Ambient temperature (°C) | 30.8 | 36.2 | 34.2 |
| Relative humidity (%) | 52 | 71 | 58.1 |
| Wind speed (km/h) | 1.3 | 6.3 | 3.9 |
| Solar irradiance (W/m²) | 323.4 | 1080.7 | 751.7 |

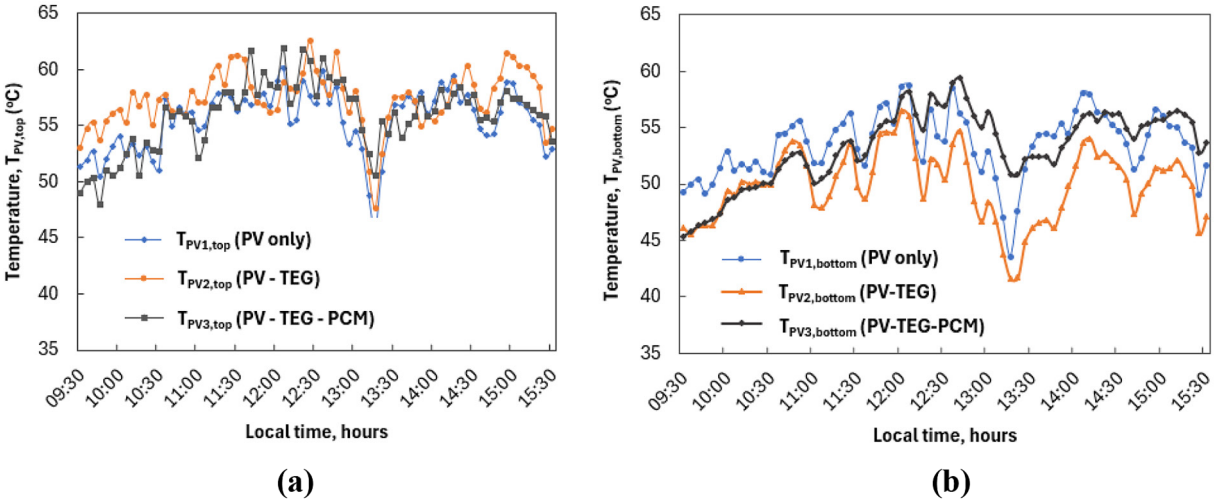



**Figure 5.** Comparison of PV surface temperatures: (a) front surface of the PV module; (b) rear surface of the PV module

Equation 4. For the PV–TEG configuration, the rear-surface $\Delta T_{PV}$ ranged from 3.5 to 10.6 °C, whereas the corresponding values for the PV–TEG–PCM configuration ranged from 0.3 to 4.3 °C. These results indicate that the reduction in rear-surface temperature was greater for the PV–TEG configuration than for the PV–TEG–PCM system. This quantitative observation is consistent with the temperature profiles presented in Figure 5, which demonstrate that incorporating PCM did not produce a greater reduction in peak temperature than the PV–TEG configuration alone. This behavior can be attributed to the additional thermal resistance introduced by the heat sink and PCM along the conductive heat transfer pathway. Consequently, although part of the thermal energy was absorbed through the latent heat storage mechanism, the overall reduction in the PV rear-surface temperature remained smaller than that achieved by the PV–TEG configuration. These findings suggest that the principal role of the PCM should not be interpreted as lowering the module temperature, but rather as regulating the rate and distribution of heat transfer within the system.

The differences in thermal response among the three configurations can be explained by changes in the heat transfer pathway. The addition of the TEG increased the thermal resistance along the conductive path toward the surrounding environment, resulting in slightly higher operating temperatures for the PV–TEG system than for the conventional PV module. In contrast, in the PV–TEG–PCM configuration, the heat sink and PCM established an additional heat transfer pathway that redirected part of the thermal energy into the latent heat storage medium (17, 25). Although this mechanism did not produce a significant reduction in the maximum module temperature, it delayed heat accumulation and consequently resulted in a more stable thermal response (3, 12). Therefore, under outdoor operating conditions, the PCM functions not as an instantaneous cooling medium but as a thermal buffer that regulates heat distribution throughout the heating process. Its primary contribution lies not in maximizing the reduction of peak temperature but in maintaining thermal stability through the temporal management of heat flow (3, 12). The observed temperature profiles indicate that this

configuration delayed the accumulation of heat on the TEG cold side and modified the transient thermal response. The contribution of latent heat storage is considered a plausible mechanism because the measured PCM temperature approached and exceeded its nominal melting temperature; however, its magnitude cannot be quantified from the present temperature measurements alone.

These findings are consistent with previous studies reporting PCM-based thermal regulation of PV systems (22, 27), including Li et al. (11) and Gürbüz et al. (3). Under the present tropical outdoor conditions, with solar irradiance reaching 1080.7 W/m² and ambient temperature 36.2 °C, PCM integration primarily improved thermal stability rather than substantially reducing peak module temperature. Therefore, thermal regulation in PV–TEG–PCM systems should be evaluated not only by peak-temperature reduction but also by the temporal evolution and distribution of heat, which directly influence the temperature gradient across the TEG and its waste-heat recovery potential (7, 13).

## Transient evolution of the TEG temperature gradient

The evolution of the temperature gradient between the hot and cold sides of the TEG during the experimental period is presented in Figure 6. For the PV–TEG configuration, the developed temperature gradient remained relatively small, ranging from approximately 1.1 to 4.3 °C, and reached a maximum of about 4.3 °C at 12:00 local time. Thereafter, the temperature gradient gradually decreased even though the PV module temperature remained relatively high. This behavior indicates that an increase in the TEG hot-side temperature does not necessarily result in a larger temperature gradient because the cold-side temperature also rises as heat accumulates, thereby progressively reducing the temperature difference across the thermoelectric module.

In contrast, the PV–TEG–PCM configuration exhibited a broader range of temperature gradients, varying from approximately 0.1 to 5.6 °C, with the maximum value occurring at approximately 10:40–10:45 local time, earlier than the time at which the PV module reached its maximum temperature. Following this peak, the temperature gradient gradually declined despite the continued increase in the TEG hot-side temperature. This behavior demonstrates that the evolution of the temperature gradient is governed not only by the hot-side temperature but also, to a large extent, by the thermal response of the cold side, which is regulated by the latent heat storage process within the PCM.

The variations in the hot-side and cold-side temperatures of the TEG are presented in Figure 7. Overall, both the PV–TEG and PV–TEG–PCM configurations exhibited temperature profiles that closely followed the fluctuations in solar irradiance throughout the experimental period. The hot-side temperature increased progressively from the beginning of the experiment, reached its maximum between approximately 12:00 and 12:30 local time, and then gradually decreased

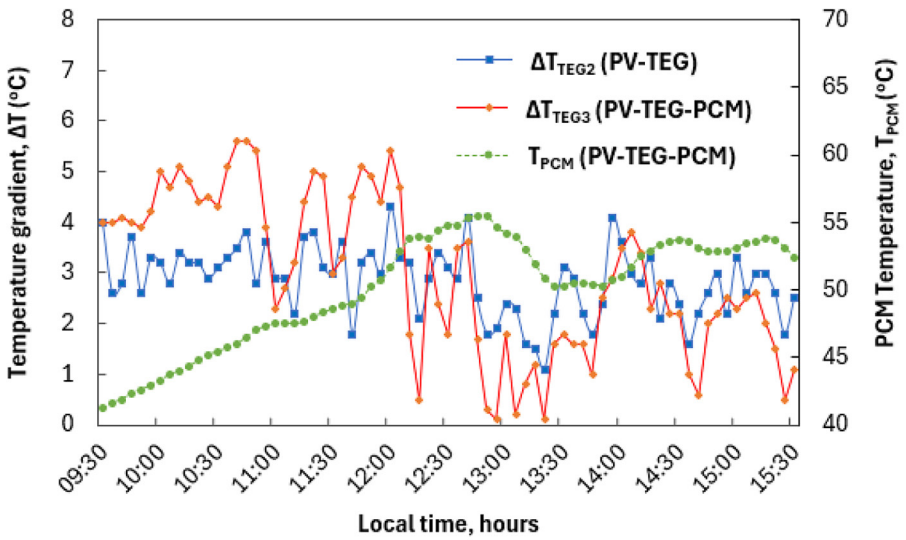



**Figure 6.** Transient temperature gradient profile of the TEG module

as solar irradiance declined. In contrast, the cold-side temperature increased at a slower rate because it was governed by the heat dissipation and thermal storage mechanisms associated with each configuration.

For the PV–TEG configuration, the hot-side temperature ranged from 41.6 to 56.5 °C, whereas the cold-side temperature varied between 40.1 and 52.7 °C. The two temperature profiles evolved almost simultaneously, indicating that the cold-side temperature increased nearly in proportion to the hot-side temperature. This behavior suggests that the heat transferred through the TEG could not be dissipated efficiently because cooling relied solely on natural convection to the surrounding environment, resulting in relatively rapid heat accumulation on the cold side.

In contrast, the PV–TEG–PCM configuration reached a higher hot-side temperature of approximately 59.4 °C, whereas the cold-side temperature increased more gradually, resulting in a larger temperature gradient during most of the heating period. This observed response indicates that the PCM modified the transient thermal pathway and delayed heat accumulation on the cold side. The behavior is consistent with thermal buffering associated with sensible and potentially latent heat storage, as reported in previous PV–TEG–PCM studies (11, 19). However, because PCM liquid fraction, heat flux, and stored latent energy were not directly measured, the contribution of latent heat storage cannot be independently quantified.

The observed difference in temperature evolution subsequently affected the TEG temperature gradient. For PV–TEG, the gradient remained relatively limited because the hot- and cold-side temperatures increased concurrently. With PCM integration, the slower cold-side response allowed a larger gradient to develop despite continued heating of the PV module. Thus, the principal observed effect of PCM was not a substantial reduction in PV temperature, but modification of the transient heat-transfer response and persistence of the temperature gradient. This interpretation is consistent with previous studies showing that PCM-based thermal management can regulate PV temperature and delay thermal accumulation under dynamic operating conditions (3, 12, 19).

To quantitatively evaluate the ability of the two hybrid configurations to sustain the temperature gradient across the TEG, two complementary thermal-gradient indicators were employed: the Effective Temperature Gradient Duration ($t_{\Delta T,eff}$) and the Cumulative Temperature Gradient Exposure (CTGE). These indicators were calculated using Equations 7 and 8, respectively. The $t_{\Delta T,eff}$ was determined using the threshold-crossing interpolation approach described in Equation 7, with $\Delta T_{th}$ = 3.0 °C. This approach accounts for the fractional portion of a 5-min measurement interval when the measured temperature-gradient curve crosses the prescribed threshold, rather than assigning the entire interval as either effective or ineffective. In addition, the cumulative TEG electrical energy ($E_{TEG}$) was calculated by integrating the measured TEG electrical power over the experimental period according to Equation 9.

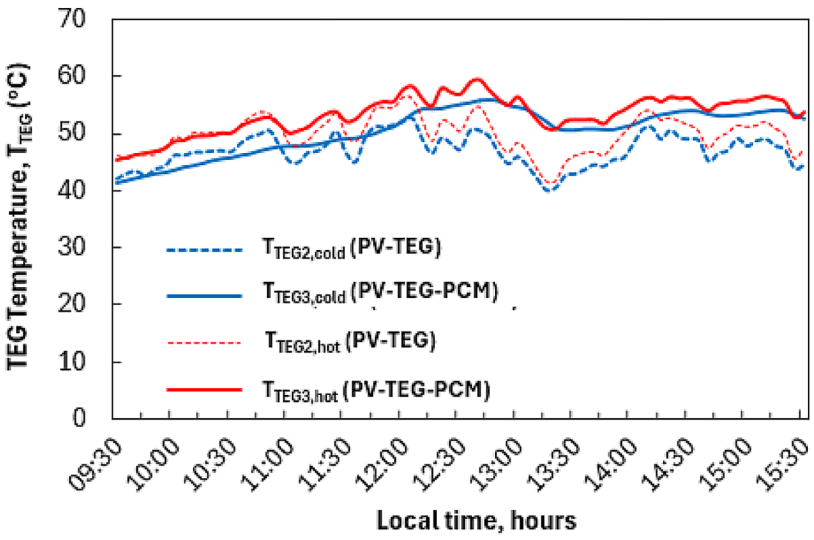



**Figure 7.** Variations in the hot-side and cold-side temperatures of the TEG

Thus, CTGE represents the cumulative thermal-gradient exposure available for thermoelectric conversion, whereas $E_{TEG}$ represents the corresponding measured electrical energy generated by the TEG. The resulting thermal-gradient indicators and cumulative TEG electrical energy are summarized in Table 5.

As shown in Table 5, the overall average temperature gradient was 2.85 ± 0.204 °C for PV–TEG and 2.91 ± 0.204 °C for PV–TEG–PCM, corresponding to an observed increase of 2.21%. This difference was smaller than the combined expanded uncertainty and therefore should not be interpreted as a resolvable enhancement in the average temperature gradient. For ΔTth = 3.0 °C, the PV–TEG–PCM configuration maintained the effective temperature gradient for 174.88 min, compared with 165.68 min for PV–TEG, an extension of 9.20 min (5.56%). This increase also remained within the combined expanded uncertainty and is therefore interpreted as an experimental trend rather than a conclusive enhancement.

The cumulative response was further characterized using the Cumulative Temperature Gradient Exposure (CTGE). CTGE increased from 1023.25 ± 13.44 °C·min for PV–TEG to 1049.75 ± 14.39 °C·min for PV–TEG–PCM, corresponding to a relative increase of 2.59%. The absolute difference was 26.50 ± 19.70 °C·min, with the combined expanded uncertainty obtained by propagating the Type-K thermocouple uncertainties through the trapezoidal integration of the 73 temperature-gradient data points; equivalently, the relative change was 2.59 ± 1.95% at k = 2. The observed CTGE increase therefore exceeded its combined expanded measurement uncertainty under the stated assumptions, indicating that the observed difference was larger than the estimated measurement uncertainty. Because the experiment involved a single measurement day without independent replicates, this comparison should not be interpreted as a statistical hypothesis test. Consistent with the CTGE result, cumulative TEG electrical energy increased from 25.02 to 25.91 J (3.56%). Thus, greater cumulative temperature-gradient exposure was accompanied by higher TEG energy generation under the tested conditions, although CTGE remains a complementary indicator rather than a direct predictor of electrical energy generation and requires validation under multiple operating days, weather conditions, PCM properties, and system configurations.

To further elucidate the transient thermal response associated with PCM integration, the temperature-gradient profiles were analyzed by dividing the experimental period into two thermal-response regimes. The first regime, termed the initial thermal-storage regime (09:30–12:50), encompasses the early heating period during which the PCM temperature increased from its initial condition toward and beyond its nominal melting temperature. This period therefore includes sensible heating and may also include progressive phase-change heat absorption. The second regime, termed the later thermal-response period (12:50–15:30), represents the subsequent period during which the temperature-gradient response declined as the PCM temperature continued to increase and the thermal-buffering effect became progressively less pronounced as the PCM temperature increased. The results of this analysis are summarized in Table 6.

As shown in Table 6, during the initial thermal-storage regime (09:30–12:50), the PV–TEG–PCM configuration exhibited an average temperature gradient of 3.98 °C, which was 25.95% higher than the 3.16 °C obtained for the PV–TEG configuration. This higher gradient indicates that the thermal response of the PCM-integrated system delayed the rise of the TEG cold-side temperature during the early heating period. Because the PCM temperature initially remained below its nominal melting temperature, this regime should not be interpreted exclusively as latent

**Table 5.** Calculated thermal-gradient indicators, expanded measurement uncertainty and cumulative TEG electrical energy

| Parameter | PV–TEG | PV–TEG–PCM | Change |
|---|---|---|---|
| Overall average ΔT (°C) | 2.85 ± 0.204 | 2.91 ± 0.204 | +2.21% |
| Effective temperature gradient duration, $t_{\Delta T,eff}$ (min) | 165.68 ± 10.01 | 174.88 ± 3.19 | +5.56% |
| Cumulative temperature gradient exposure (CTGE) (°C·min) | 1023.25 ± 13.44 | 1049.75 ± 14.39 | +26.50 ± 19.70 (+2.59 ± 1.95%) |
| Cumulative TEG electrical energy ($E_{TEG}$) (J) | 25.02 | 25.91 | +3.56% |

**Table 6.** Comparison of the average TEG temperature gradient during two thermal-response regimes

| Operating stage | Duration | Average ΔT PV–TEG | Average ΔT PV–TEG–PCM | Change |
|---|---|---|---|---|
| | (min) | (°C) | (°C) | (%) |
| Initial thermal-storage regime (09:30–12:50) | 200 | 3.16 | 3.98 | 25.95% |
| Later thermal-response period (12:50-15:30) | 160 | 2.48 | 1.62 | -34.68% |

heat storage; rather, it represents a combined sensible-heating and thermal-storage response, with phase-change heat absorption potentially contributing as the PCM approached and exceeded its nominal melting temperature. This interpretation remains qualitative because the phase fraction and latent energy storage were not directly measured. During the later thermal-response period (12:50–15:30), the average temperature gradients were 2.48 °C for PV–TEG and 1.62 °C for PV–TEG–PCM. The lower gradient observed for PV–TEG–PCM during this period indicates that the thermal advantage associated with the earlier storage process diminished as the PCM temperature increased and its available thermal-storage capacity was progressively reduced. Since the present experiment did not independently determine the phase-change onset and completion temperatures, these two time periods are interpreted as thermal-response regimes rather than direct measurements of the PCM phase-change interval.

Overall, the results demonstrate that the principal contribution of the PCM is not to increase the maximum temperature gradient but rather to extend the duration and increase the cumulative exposure to an effective temperature gradient during transient operation. This conclusion is consistently reflected by the improvements in both the effective temperature gradient duration and the CTGE, which together characterize the persistence of the thermal driving force throughout the experimental period. Accordingly, these two parameters provide complementary information for assessing waste heat recovery performance under transient operating conditions. Accordingly, the combined use of effective temperature gradient duration and CTGE is proposed as a complementary evaluation approach for characterizing transient thermal-gradient persistence and cumulative exposure alongside conventional instantaneous performance metrics.

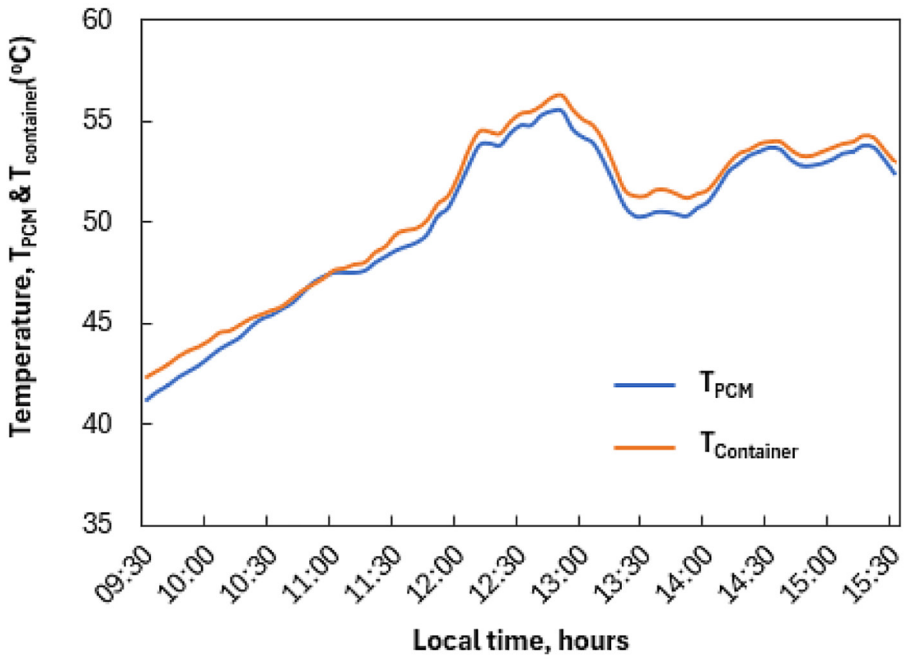



**Figure 8.** Evolution of the PCM temperature and the temperature of the outer bottom surface of the aluminum PCM container during the experimental period

## Thermal storage behaviour of PCM and heat transfer mechanism

The evolution of the PCM temperature and the temperature of the outer bottom surface of the PCM container during the experimental period is presented in Figure 8, while the relationship among the PCM temperature, the rear surface temperature of the PV module, and the TEG temperature gradient (ΔT) is illustrated in Figure 9. The PCM temperature increased gradually from approximately 41.2 to 55.5 °C, whereas the outer wall temperature of the container increased from 42.3 to 56.3 °C. Both temperatures exhibited similar temporal evolution with only a small temperature difference throughout the experiment, indicating close thermal coupling and continuous heat transfer through the thin aluminum container wall. The outer bottom surface was covered by thermal insulation, which provided thermal isolation from the surrounding environment and limited external heat exchange. However, because heat flux was not directly measured and a complete energy balance was not performed, the magnitude of environmental heat loss cannot be quantified from the present temperature measurements. The measured temperature evolution provides evidence of the thermal-storage and buffering response of the PCM-integrated system. Nevertheless, the present experiment did not directly measure PCM liquid fraction, heat flux, stored thermal energy, or calorimetric phase-change characteristics. Therefore, the temperature profiles alone cannot be used to quantitatively determine the amount of latent heat absorbed or the exact progression and completion of the phase-change process. The observed response is consequently interpreted as a combined thermal-storage effect, with latent heat absorption considered a plausible contributing mechanism as the PCM temperature approached and exceeded its nominal melting temperature.

Compared with the rear surface temperature of the PV module, the PCM temperature increased at a considerably slower rate throughout the experiment. As the rear surface temperature of the PV module rose rapidly in response to increasing solar irradiance, the PCM exhibited a more gradual thermal response. This difference in heating rate indicates a thermal-storage and buffering response of the PCM. Because the PCM liquid fraction and heat flux were not directly measured, the respective sensible and latent heat contributions cannot be quantitatively separated. This behavior is also evident in Figure 9, where the TEG temperature gradient reached its maximum value while the PCM temperature remained relatively low and subsequently declined gradually as the PCM temperature increased during the thermal energy storage process. These observations indicate that the evolution of ΔT is governed primarily by the ability of the PCM to absorb and delay heat transfer rather than solely by the increase in PV module temperature.

Figure 9 further illustrates the relationship between PCM temperature, PV rear-surface temperature, and TEG temperature gradient. The

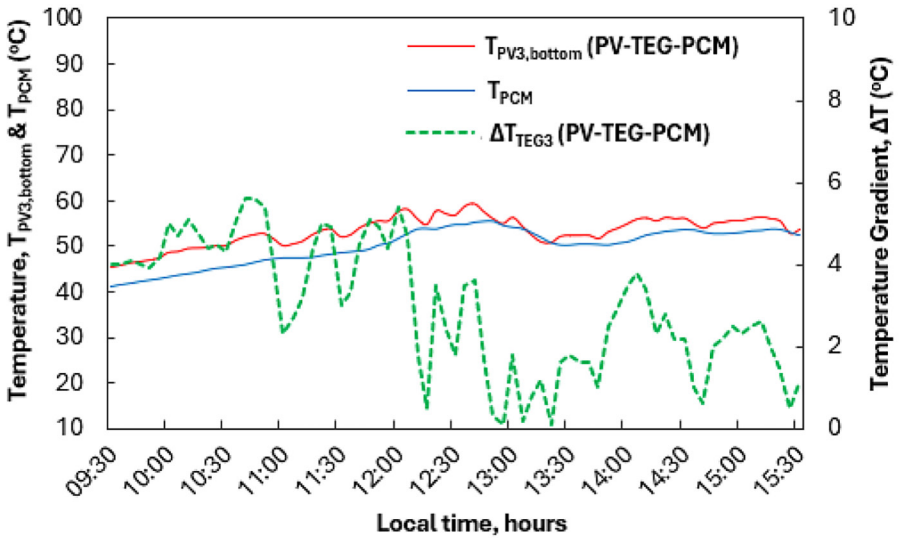



**Figure 9.** Relationship between PCM temperature, PV rear-surface temperature, and TEG temperature gradient in the PV-TEG-PCM system

PCM temperature increased more gradually than the PV rear-surface temperature, while the TEG temperature gradient reached its maximum before subsequently declining as the PCM temperature continued to rise. This response indicates that PCM integration modified the transient thermal response and delayed the increase in the TEG cold-side temperature. The observed behavior is consistent with thermal buffering associated with sensible and potentially latent heat storage reported in previous studies (11, 19). However, because PCM liquid fraction, heat flux, and stored latent energy were not directly measured, the contribution of latent heat storage cannot be independently quantified.

The results indicate that the benefit of PCM was primarily associated with the persistence of a favorable temperature gradient rather than a substantial reduction in PV temperature. Accordingly, the transient response was further quantified using the Effective Temperature Gradient Duration and CTGE, which characterize the persistence and cumulative exposure of the measured TEG temperature gradient, respectively (4, 23).

## Electrical performance of photovoltaic modules

The relationship between solar irradiance and the electrical power output of the PV modules is presented in Figure 10. All three configurations exhibited a similar trend, with the electrical power increasing as solar irradiance intensified from the morning until around midday, followed by a gradual decline as solar irradiance decreased in response to changing weather conditions. This behavior confirms that solar irradiance remained the dominant factor governing the electrical output of the PV modules across all investigated configurations.

For the conventional PV configuration, the measured electrical power delivered to the fixed load ranged from 1.25 to 16.53 W, with an output voltage of 4.05–16.13 V and an output current of 0.270–1.075 A. The PV–TEG configuration produced measured electrical power of 1.49–22.84 W, with voltages between 4.72 and 18.51 V and currents between 0.315 and 1.234 A. Meanwhile, the PV–TEG–PCM configuration generated 1.34–16.98 W, with an output voltage of 4.21–16.39 V and an output current of 0.281–1.093 A. These values represent the electrical power delivered to the fixed 15 Ω load under transient outdoor conditions rather than maximum power-point values.

Before interpreting the differences in the measured PV power, the initial electrical comparability of the three PV modules was evaluated using the pre-modification baseline measurements. The baseline test was conducted simultaneously under the same outdoor conditions using the same measurement system and the same 15 Ω–100 W resistive load. In the baseline dataset, the mean electrical powers of $PV_1$, $PV_2$, and $PV_3$ were 3.34, 3.19, and 3.19 W, respectively. These values correspond to deviations of +3.09%, −1.60%, and −1.49%, respectively, from the three-module

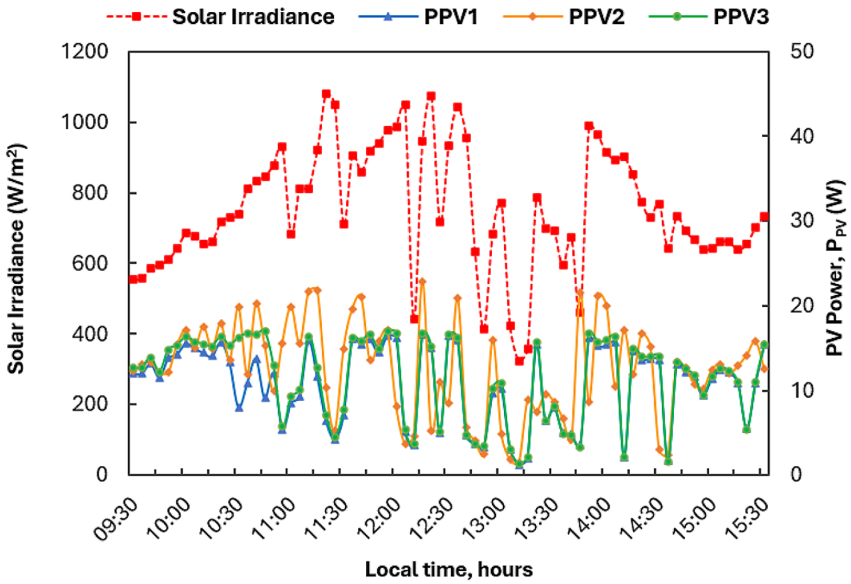



**Figure 10.** Relationship between solar irradiance and PV power output

grand mean of 3.239 W. The corresponding baseline correction factors were 0.97, 1.02, and 1.01 for $PV_1$, $PV_2$, and $PV_3$, respectively. The proximity of these factors to unity indicates that the three modules exhibited closely comparable initial electrical responses before physical modification.

The measured PV power obtained during the main experiment was subsequently normalized using these module-specific baseline correction factors. The highest baseline-normalized measured PV electrical powers were 16.03 W, 23.21 W, and 17.24 W for the PV, PV–TEG, and PV–TEG–PCM configurations, respectively, compared with the corresponding measured peak values of 16.53 W, 22.84 W, and 16.98 W. The relatively small changes following baseline normalization indicate that the differences in the initial electrical characteristics of the three PV modules were insufficient to account for the observed differences in instantaneous peak power.

Thus, the measured highest values of 16.53, 22.84, and 16.98 W represent the instantaneous peak power output exerted to a fixed load under the transient outdoor conditions of the experiment, not the maximum power point value. The interpretation should take into account the simultaneous variations between solar irradiation, PV operating temperature, and electrical operating conditions imposed by fixed resistive loads.

These differences are closely associated with the heat transfer mechanisms operating within each configuration. From a theoretical perspective, increasing solar irradiance enhances the generation of electron–hole pairs, thereby increasing the photocurrent, whereas higher operating temperatures reduce the output voltage because of enhanced charge-carrier recombination and a decrease in the open-circuit voltage. In the PV–TEG configuration, the presence of the TEG introduces additional thermal resistance at the rear surface of the PV module, causing the operating temperature to increase when heat cannot be dissipated effectively from the cold side. In contrast, in the PV–TEG–PCM configuration, the PCM absorbs part of the incoming thermal energy through latent heat storage, slowing the rate of temperature increase and resulting in a more gradual thermal response of the PV module. Consequently, fluctuations in output voltage and measured electrical power may become less pronounced, although the highest measured electrical output does not show a substantial increase.

The effect of PCM integration should not be evaluated solely from the instantaneous peak PV electrical output. Instead, its potential benefit is more appropriately considered in terms of thermal buffering and the resulting stability of PV operating conditions under transient thermal loads. By moderating the rate of PV temperature variation, the PCM can contribute to a more gradual thermal response of the PV–TEG–PCM configuration. Accordingly, the effectiveness of the PV–TEG–PCM system is better assessed from its transient thermal regulation and electrical response over the operating period rather than from the absolute peak power alone.

These observations are consistent with previous studies reporting that PCM integration can improve the electrical performance of photovoltaic systems through module temperature regulation (18, 23). However, most of these studies were conducted using numerical simulations or laboratory experiments under relatively constant irradiance conditions (22, 27). In contrast, the present results demonstrate that under tropical outdoor conditions characterized by substantial fluctuations in solar irradiance, the principal benefit of PCM lies in maintaining the stability of electrical output rather than increasing instantaneous power generation. This interpretation is consistent with the observations reported by Li et al. (11) and Darkwa et al. (21), who likewise found that thermal regulation provided by PCM resulted in a more stable electrical response during transient operation.

Overall, the present study demonstrates that the maximum PV module temperature is not the sole parameter governing the electrical performance of photovoltaic systems. The ability of the system to control temperature dynamics through heat flow management and thermal energy storage can contribute significantly to the stability of the electrical output under transient operating conditions. Accordingly, the performance enhancement achieved by the PV–TEG–PCM system can be attributed to the interaction among thermal regulation, heat flow management, and waste heat utilization through thermoelectric energy conversion, consistent with recent experimental investigations of hybrid PV–TEG–PCM systems (3, 19).

## Waste heat recovery performance of the thermoelectric generator

In the PV–TEG–PCM system, thermal energy not converted into electricity by the PV module is utilized as the heat source for the TEG.

Accordingly, waste heat recovery was evaluated from the TEG output voltage, electrical power, and contribution to the total system power. The transient TEG voltage and power are presented in Figure 11. For the PV–TEG configuration, the output voltage ranged from 0.05 to 0.16 V, and the highest measured electrical power was 2.56 mW. After PCM integration, the voltage increased to approximately 0.21 V and the highest measured electrical power reached 4.24 mW, corresponding to a relative increase of 65.77% and an absolute increase of 1.68 mW. However, this relative increase should be interpreted in the context of the overall system output, as the TEG contribution remained below 0.06% of the total electrical power. Thus, the 65.77% increase represents a relative improvement in measured TEG output under the tested transient conditions rather than a substantial increase in the overall electrical energy production of the PV system.

The relative contribution of the TEG to the total system power ($C_{TEG}$) was calculated using Equation (6). For the PV–TEG configuration, $C_{TEG}$ ranged from 0.003 to 0.054%, whereas for the PV–TEG–PCM configuration it varied between 0.0001 and 0.054%. The nearly identical maximum values obtained for both configurations indicate that the electrical output of the TEG remained fundamentally constrained by the temperature gradient that could be established during the experiment. Nevertheless, the broader variation in $C_{TEG}$ observed for the PV–TEG–PCM configuration reflects a more dynamic response to changing thermal conditions resulting from the charging and discharging processes of the PCM. Although the contribution of the TEG accounted for less than 0.06% of the total system power, the $C_{TEG}$ parameter is consistent with that a portion of the thermal energy previously dissipated as waste heat was successfully converted into electrical energy through the waste heat recovery process. Accordingly, an increase in $C_{TEG}$ should be interpreted primarily as an indicator of waste heat utilization through thermoelectric conversion rather than as a substantial increase in the overall electrical output of the system.

Figure 12 presents the relationship between the measured temperature gradient ($\Delta T$) and TEG electrical power output for the PV–TEG and PV–TEG–PCM configurations. For the PV–TEG configuration, most data points were concentrated within a $\Delta T$ range of approximately 2–4 °C, with measured TEG power ranging from 0.25 to 2.56 mW. The second-order polynomial fit showed an overall increase in power with increasing $\Delta T$, although the relatively low coefficient of determination ($R^2$ = 0.2745) indicates that $\Delta T$ alone provides limited explanation of instantaneous power variation under the transient outdoor conditions. In contrast, the PV–TEG–PCM configuration exhibited a broader $\Delta T$ range, reaching approximately 5.6 °C, with a peak measured TEG power of 4.24 mW. Its second-order polynomial fit yielded $R^2$ = 0.4794, indicating a comparatively stronger empirical association between $\Delta T$ and instantaneous TEG power, although substantial scatter remained.

The broader $\Delta T$ distribution observed with PCM integration reflects the different transient thermal response of the system. Under idealized conditions with an approximately constant Seebeck coefficient, fixed internal and load resistance,

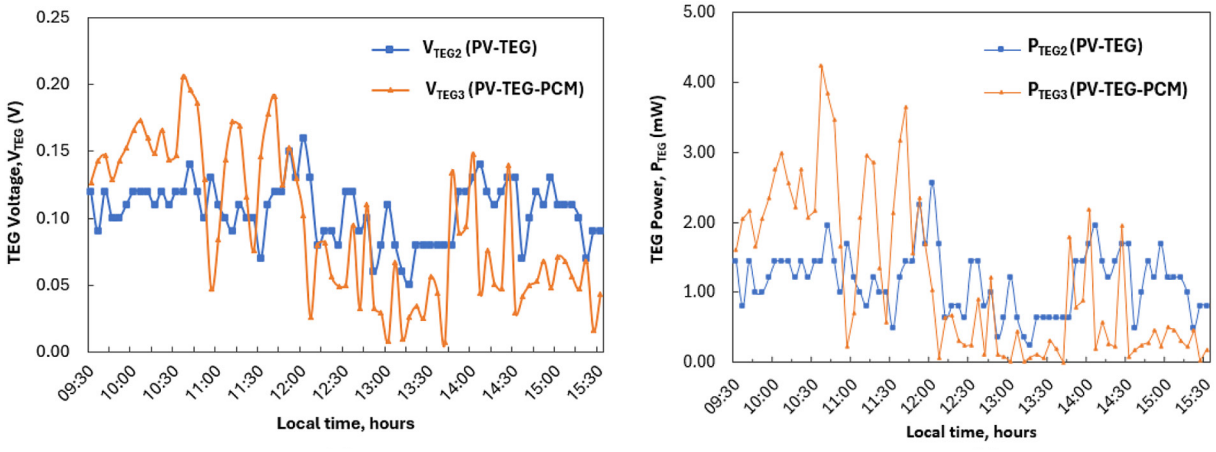



**Figure 11.** (a) TEG output voltage; (b) TEG electrical power output

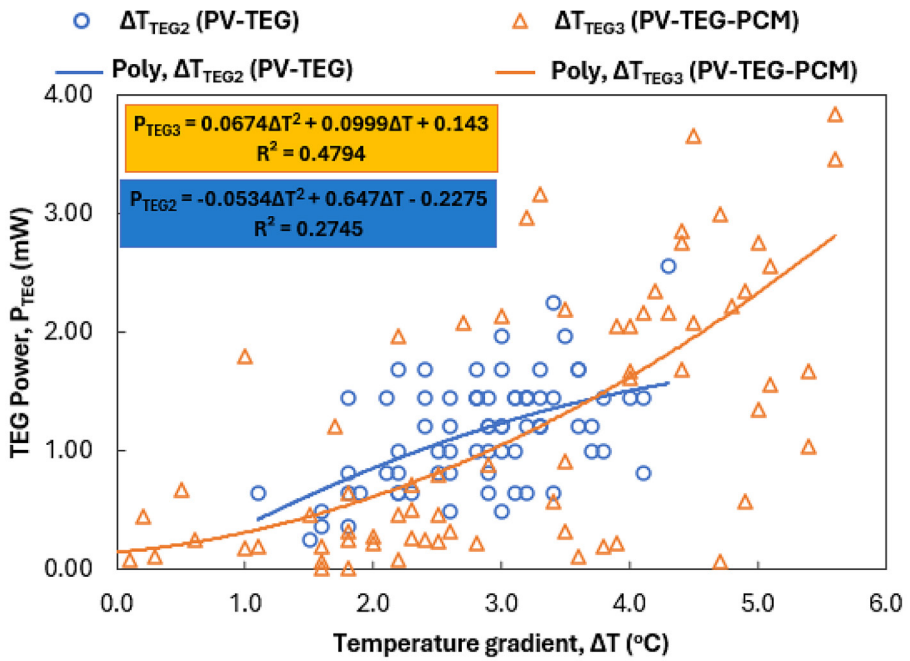



**Figure 12.** Empirical relationship between the measured TEG temperature gradient ($\Delta T$) and electrical power output under the fixed electrical load

TEG voltage is approximately proportional to $\Delta T$, resulting in an approximately quadratic dependence of electrical power on $\Delta T$. However, the measured outdoor response is also affected by transient thermal conditions, temperature-dependent thermoelectric properties, thermal-interface effects, and other operating variations. Therefore, the second-order polynomial fits in Figure 12 are interpreted as empirical descriptions of the measured data rather than universal or predictive thermoelectric relationships**.**

The increase in TEG power output did not always correspond directly to increasing solar irradiance. Instead, the highest measured TEG electrical power was obtained when the temperature gradient (ΔT) reached its optimum value, demonstrating that ΔT is a primary thermal parameter governing the measured TEG power under the fixed electrical load used in this study, whereas the absolute temperature of the PV module serves only as the thermal energy source. This behavior can be explained by the transient heat transfer process. During the initial stage of operation, the high latent heat storage capacity of the PCM delayed the increase in cold-side temperature, allowing the temperature gradient to develop progressively. As the PCM temperature increased, the thermal-buffering effect became less pronounced, as indicated by the progressive increase in cold-side temperature and the corresponding decline in ΔT. This behavior is interpreted as a temperature-based indication of reduced thermal buffering rather than direct evidence of complete PCM saturation. Therefore, the improvement in TEG electrical output does not arise from changes in the intrinsic characteristics of the thermoelectric module but rather from more effective management of heat distribution that sustains favorable thermal conditions for energy conversion.

These findings are consistent with previous studies reporting that a larger temperature gradient (ΔT) leads to higher TEG electrical output (11, 19), and that PCM enhances thermoelectric performance by regulating the cold-side temperature (3, 23). However, most of these studies were based on numerical simulations or laboratory experiments conducted under steady-state conditions and primarily evaluated performance using the highest measured power output under the fixed load (22, 27). In contrast, the present experimental results demonstrate that the improvement in electrical output is a direct consequence of the system's ability to sustain the temperature gradient under transient operating conditions. This interpretation is consistent with the observations reported by Darkwa et al., Rajaee et al., and Okamkpa et al., who emphasized the importance of the cold-side heat transfer configuration in maintaining thermoelectric energy conversion

performance (8, 21, 30). From a scientific perspective, these findings demonstrate that waste heat recovery in PV–TEG–PCM systems is governed more by the quality of thermal management than by the amount of waste heat available. The observed increase in TEG power output is consistent with a role of PCM integration in regulating the thermal boundary conditions and sustaining favorable temperature-gradient conditions.

## CONCLUSIONS

The experimental results demonstrate that PCM integration modified the transient thermal response of the PV–TEG system by delaying the rise of the TEG cold-side temperature and sustaining a favorable temperature gradient for longer under the tested outdoor conditions. The observed response is consistent with combined sensible and potentially latent heat storage; however, because PCM liquid fraction, heat flux, stored latent energy, and calorimetric phase-change characteristics were not directly measured, the contribution of latent heat storage cannot be quantitatively separated from the overall thermal-storage response. The maximum TEG temperature gradient increased from approximately 4.3 to 5.6 °C, corresponding to a 65.77% increase in peak TEG power from 2.56 to 4.24 mW. Nevertheless, the absolute increase was only 1.68 mW, and the TEG contribution remained below 0.06% of the total electrical output, indicating that the practical system-level electrical contribution remained limited.

The results further show that TEG performance was governed primarily by the transient evolution of the temperature gradient rather than by the maximum PV temperature alone. The effective temperature gradient duration increased from 165.68 to 174.88 min (5.56%), while CTGE increased from 1023.25 to 1049.75 °C·min (2.59%). The increase in CTGE was accompanied by an increase in measured cumulative TEG electrical energy from 25.02 to 25.91 J (3.56%), supporting the physical relevance of CTGE as a complementary indicator of cumulative thermal-gradient exposure associated with TEG energy recovery. However, CTGE should not be interpreted as a direct predictor of electrical energy generation. The average temperature gradient was 25.95% higher in the PV–TEG–PCM configuration during the initial thermal-storage regime, but 34.68% lower during the later thermal-response period, indicating that the thermal-buffering benefit was transient and became less pronounced as the PCM temperature increased.

Overall, the effective temperature gradient duration and CTGE are proposed as complementary indicators for characterizing thermal-gradient persistence and cumulative exposure under transient outdoor conditions, rather than as universally superior performance metrics. The findings are based on a single-day, six-hour outdoor experiment and therefore should be interpreted within the specific boundary conditions tested. Broader applicability requires validation through multi-day experiments, different weather conditions, PCM properties, and system configurations. Future optimization should focus on PCM thermal characteristics, heat sink geometry, thermal contact resistance, insulation, and TEG configuration to extend the effective temperature-gradient duration and improve waste-heat recovery.

## REFERENCES

1. Buyukbicakci E. Geographic and thermal impact on the performance of hybrid PV–TE energy systems. Sci Rep [Internet]. 2025 Nov 17; 15(1): 40169. https://doi.org/10.1038/s41598-025-23850-x
2. Cui Y, Zhu J., Zhang F, Shao Y, Xue Y. Current status and future development of hybrid PV/T system with PCM module: 4E (energy, exergy, economic and environmental) assessments. Renew Sustain Energy Rev. 2022 Apr; 158: 112147. https://doi.org/10.1016/j.rser.2022.112147
3. Gürbüz H, Demirtürk S, Akçay H, Topalcı Ü. Thermal stabilization and energy harvesting in a solar PV/T-PCM-TEG hybrid system: A case study on the design of system components. Energy Convers Manag. 2023; 294. https://doi.org/10.1016/j.enconman.2023.117536
4. Vaziri Rad MA, Rousta M, Khanalizadeh A, Kouravand A, Akbari M, Mousavi S, et al. Critical analysis of enhanced photovoltaic thermal systems: a comparative experimental study of PCM, TEG, and nanofluid applications. Energy Convers Manag. 2024;314. https://doi.org/10.1016/j.enconman.2024.118712
5. Rejeb O, Lamrani B, Lamba R, Kousksou T, Salameh T, Jemni A, et al. Numerical investigations of concentrated photovoltaic thermal system integrated with thermoelectric power generator and phase change material. J Energy Storage. 2023; 62. https://doi.org/10.1016/j.est.2023.106820
6. Khan A, Shahzad N, Waqas A, Mahmood M, Ali M,

Umar S. Unlocking the potential of passive cooling: A comprehensive experimental study of PV/PCM/TEC hybrid system for enhanced photovoltaic performance. J Energy Storage. 2024; 80(December 2023). https://doi.org/10.1016/j.est.2023.110277

7. Wei W, Li N, Che L, Fan Y, Liu H, Ji J, et al. A continuous 24-hour power generated PV-TEG-PCM hybrid system enabled by solar diurnal photovoltaic/thermal conversion and nocturnal sky radiative cooling. Energy Convers Manag. 2024; 321. https://doi.org/10.1016/j.enconman.2024.119086
8. Rajaee F, Rad MAV, Kasaeian A, Mahian O, Yan WM. Experimental analysis of a photovoltaic/thermoelectric generator using cobalt oxide nanofluid and phase change material heat sink. Energy Convers Manag. 2020 May; 212: 112780. https://doi.org/10.1016/j.enconman.2020.112780
9. Alkhalil S, Altork Y, Sukkariyh M, Abdelhafez E. Enhancing photovoltaic panel performance through hybrid nanoparticle cooling – a study on zinc oxide and aluminum oxide nanofluids. Adv Sci Technol Res J. 2024; 18(4): 329–35.
10. Płachta K, Mroczka J, Ostrowski M. A new approach to water cooling of photovoltaic panels with a tracking system. Metrol Meas Syst. 2023; 30(4): 675–87.
11. Li T, Yu J, Peng X, Zhou W, Xu C, Li G, et al. Comparison of the thermoelectric performance of different photovoltaic/thermal hybrid thermoelectric generation modules: An experimental study. Appl Energy. 2025 Jan; 378: 124771. https://doi.org/10.1016/j.apenergy.2024.124771
12. Bhutto YA, Pandey AK, Saidur R, Rathore PKS, Samykano M. Hybrid silver-graphene nanoparticles enhanced Lauric Acid phase change material for photovoltaic and thermoelectric generator applications: Experimental and simulation analysis. J Energy Storage. 2024; 93(5). https://doi.org/10.1016/j.est.2024.112320
13. Alghamdi H, Maduabuchi C, Mbachu DS, Albaker A, Alatawi I, Alsenani TR, et al. Machine learning model for transient exergy performance of a phase change material integrated-concentrated solar thermoelectric generator. Appl Therm Eng. 2023;228(March). https://doi.org/10.1016/j.applthermaleng.2023.120540
14. Adhitya DC, Rahmalina D, Ismail, Alphanoda AF, Rahman RA. Assessment of thermal behavior for phase transition material through dynamic heating-cooling scenario energy system. Adv Sci Technol Res J. 2026; 20(9): 411–23.
15. Lamba R, Montero FJ, Rehman T, Singh S, Manikandan S. PCM-based hybrid thermal management system for photovoltaic modules: A comparative analysis. Environ Sci Pollut Res. 2023 Jun 5; 31(34): 46397–416. https://doi.org/10.1007/s11356-023-27809-1
16. Win SLY, Chiang Y-C, Huang T-L, Lai C-M. Thermoelectric generator applications in buildings: A review. Sustainability. 2024 Sep 2; 16(17): 7585. https://doi.org/10.3390/su16177585
17. Cui T, Xuan Y, Li Q. Design of a novel concentrating photovoltaic-thermoelectric system incorporated with phase change materials. Energy Convers Manag. 2016; 112: 49–60. https://doi.org/10.1016/j.enconman.2016.01.008
18. Naderi M, Ziapour BM, Gendeshmin MY. Improvement of photocells by the integration of phase change materials and thermoelectric generators (PV-PCM-TEG) and study on the ability to generate electricity around the clock. J Energy Storage. 2021; 36(December 2020). https://doi.org/10.1016/j.est.2021.102384
19. Maleki Y, Pourfayaz F, Mehrpooya M. Experimental study of a novel hybrid photovoltaic/thermal and thermoelectric generators system with dual phase change materials. Renew Energy. 2022; 201(P2): 202–15. https://doi.org/10.1016/j.renene.2022.11.037
20. Khan MAI, Khan MI, Kazim AH, Shabir A, Riaz F, Mustafa N, et al. An experimental and comparative performance evaluation of a hybrid photovoltaic-thermoelectric system. Front Energy Res. 2021; 9(September): 1–9. https://doi.org/10.3389/fenrg.2021.722514
21. Darkwa J, Calautit J, Du D, Kokogianakis G. A numerical and experimental analysis of an integrated TEG-PCM power enhancement system for photovoltaic cells. Appl Energy. 2019; 248: 688–701. https://doi.org/10.1016/j.apenergy.2019.04.147
22. Lv S, Yang J, Ren J, Zhang B, Lai Y, Chang Z. Research and numerical analysis on performance optimization of photovoltaic-thermoelectric system incorporated with phase change materials. Energy. 2023; 263. https://doi.org/10.1016/j.energy.2022.125850
23. Lv S, Liu W, Yang J. Performance optimization of photovoltaic thermoelectric systems based on phase change materials. Renew Energy. 2025; 240(June 2024): 122203. https://doi.org/10.1016/j.renene.2024.122203
24. Soliman AMA, Yousef MS, Ookawara S, Hassan H. Experimental study of using system of flat heat pipe-phase change material inclusion heat sink for thermal regulation of simulated PV. Exp Heat Transf. 2023; 36(5): 648–64. https://doi.org/10.1080/08916152.2022.2071359
25. Khoshnazm MJ, Marzban A, Azimi N. Performance enhancement of photovoltaic panels integrated with thermoelectric generators and phase change materials: Optimization and analysis of thermoelectric

arrangement. Energy. 2023; 267(December 2022). https://doi.org/10.1016/j.energy.2022.126556

26. Ko J, Jeong JW. Annual performance evaluation of thermoelectric generator-assisted building-integrated photovoltaic system with phase change material. Renew Sustain Energy Rev. 2021;145(April). https://doi.org/10.1016/j.rser.2021.111085
27. Motiei P, Yaghoubi M, GoshtasbiRad E. Transient simulation of a hybrid photovoltaic-thermoelectric system using a phase change material. Sustain Energy Technol Assessments. 2019; 34(May): 200–13. https://doi.org/10.1016/j.seta.2019.05.004
28. Chapra SC, Canale RP. Numerical Methods For Engineers. Sixth. New York: McGraw-Hill;
29. Burden RL, Faires JD. Numerical Analysis. Ninth. Julet M, editor. Boston: Richard Stratton; 2001.
30. Okamkpa T, Okechukwu J, Mbachu D, Mgbemene C. Performance analysis of a photovoltaic system with thermoelectric generator and phase change material: An experimental approach. Adv Sci Technol. 2025; 160: 53–63. https://doi.org/10.4028/p-AK81Yk